# MOUNTAIN-PLAINS CONSORTIUM

**MPC 23-505** | G. Hou and S. Chen

## MODELING DISRUPTED TRANSPORTATION INFRASTRUCTURE SYSTEM DUE TO FALLEN TREES UNDER WIND HAZARDS

MOUNTAIN-PLAINS CONSORTIUM REGION 8

A University Transportation Center sponsored by the U.S. Department of Transportation serving the Mountain-Plains Region. Consortium members:

Colorado State University
North Dakota State University
South Dakota State University
University of Colorado Denver
University of Denver
University of Utah
Utah State University
University of Wyoming

**Technical Report Documentation Page**

| 1. Report No. | 2. Government Accession No. | 3. Recipient's Catalog No. |
|---|---|---|
| MPC-617 | | |

| 4. Title and Subtitle | 5. Report Date |
|---|---|
| Modeling Disrupted Transportation Infrastructure System due to Fallen Trees under Wind Hazards | September 2023 |
| | 6. Performing Organization Code |

| 7. Author(s) | 8. Performing Organization Report No. |
|---|---|
| Suren Chen<br>Guangyang Hou | MPC 23-505 |

| 9. Performing Organization Name and Address | 10. Work Unit No. (TRAIS) |
|---|---|
| Colorado State University<br>1372 Campus Delivery<br>Fort Collins, CO 80523 | 11. Contract or Grant No. |

| 12. Sponsoring Agency Name and Address | 13. Type of Report and Period Covered |
|---|---|
| Mountain-Plains Consortium<br>North Dakota State University<br>PO Box 6050, Fargo, ND 58108 | Final Report |
| | 14. Sponsoring Agency Code |

15. Supplementary Notes

Supported by a grant from the US DOT, University Transportation Centers Program

16. Abstract

Tree failures due to strong winds in urban areas cause extensive direct and indirect economic and environmental loss, including disrupting adjacent infrastructures, such as buildings, underground pipelines, roads, and overhead powerlines. To effectively improve the resilience of a community subjected to extreme wind events through prevention, response, and recovery, it becomes critical to rationally assess the risks of wind-induced tree failures and the disruptions to different types of infrastructures due to fallen trees. An integrated probabilistic methodology to model the performance of disrupted infrastructures is developed for fallen urban trees subjected to extreme winds in a typical community. First, the finite-element modeling of the trees subjected to wind loads is conducted and, based on which, the windthrow fragility curves of several typical urban tree species are developed. Second, a probabilistic framework is developed based on the fragility results to characterize the disrupted scenarios and further predict the disruption probability of some critical infrastructures due to fallen trees. The matrix-based system reliability (MSR) method is introduced to assess the transportation network performance. The proposed framework and MSR method are demonstrated in detail while studying the overhead powerline and transportation network of a small urban community in the city of Fort Collins, Colorado. In the demonstrative example, the probabilities of powerline disruption, road closure, and origin-destination (OD) disconnection and travel time reliability under different wind conditions are predicted. Finally, mitigation efforts such as crown thinning of trees are discussed to reduce possible risks of disrupting the infrastructures.

| 17. Key Word | 18. Distribution Statement |
|---|---|
| Bridges, forecasting, hazards, highways, rural areas, service disruption, traffic incidents, travel time, urban areas | Public distribution |

| 19. Security Classif. (of this report) | 20. Security Classif. (of this page) | 21. No. of Pages | 22. Price |
|---|---|---|---|
| Unclassified | Unclassified | 37 | n/a |

**Form DOT F 1700.7 (8-72)** Reproduction of completed page authorized

# Modeling Disrupted Transportation Infrastructure System due to Fallen Trees under Wind Hazards

Guangyang Hou
Suren Chen

Department of Civil and Environmental Engineering
Colorado State University
Fort Collins, CO 80523

September 2023

## Acknowledgement

The funds for this study were provided by the United States Department of Transportation to the Mountain Plains Consortium (MPC).

## Disclaimer

# ABSTRACT[1]

Tree failures due to strong winds in urban areas cause extensive direct and indirect economic and environmental loss, including disrupting adjacent infrastructures, such as buildings, underground pipelines, roads, and overhead powerlines. To effectively improve the resilience of a community subjected to extreme wind events through prevention, response, and recovery, it becomes critical to rationally assess the risks of wind-induced tree failures and the disruptions to different types of infrastructures due to fallen trees. An integrated probabilistic methodology to model the performance of disrupted infrastructures is developed for fallen urban trees subjected to extreme winds in a typical community. First, the finite-element modeling of the trees subjected to wind loads is conducted and, based on which, the windthrow fragility curves of several typical urban tree species are developed. Second, a probabilistic framework is developed based on the fragility results to characterize the disrupted scenarios and further predict the disruption probability of some critical infrastructures due to fallen trees. The matrix-based system reliability (MSR) method is introduced to assess the transportation network performance. The proposed framework and MSR method are demonstrated in detail while studying the overhead powerline and transportation network of a small urban community in the city of Fort Collins, Colorado. In the demonstrative example, the probabilities of powerline disruption, road closure, and origin-destination (OD) disconnection and travel time reliability under different wind conditions are predicted. Finally, mitigation efforts such as crown thinning of trees are discussed to reduce possible risks of disrupting the infrastructures.

[1] This report is based on the contents from the published journal paper: Hou, G., and Chen, S. (2020). "Probabilistic modeling of disrupted infrastructures due to fallen trees subjected to extreme winds in urban community," *Natural Hazards*, 102: 1323-1350.

# TABLE OF CONTENTS

**1. INTRODUCTION AND LITERATURE REVIEW ..... 1**
1.1 Background ..... 1
1.2 Organization of Report ..... 2

**2. FRAGILITY MODEL OF URBAN TREES SUBJECTED TO EXTREME WINDS ..... 3**
2.1 Description of Urban Trees ..... 3
2.2 Mechanistic Tree Model ..... 5
2.2.1 Wind Loads ..... 5
2.2.2 Self-weight ..... 6
2.2.3 Application of Direct Stiffness Method ..... 6
2.3 Limit State ..... 8
2.4 Statistics of Wind Loads and Mechanical Properties of Trees ..... 8
2.5 Development of Fragility Curves ..... 9

**3. PROBABILISTIC METHDOLOGY OF MODELING DISRUPTED INFRASTRUCTURE DUE TO FALLEN TREES ..... 16**
3.1 Probabilistic Model of Infrastructure Disruption ..... 16
3.2 Transportation Network Analysis in Emergency Response Stage ..... 18
3.2.1 Connectivity Analysis ..... 18
3.2.2 Travel Time Reliability Analysis ..... 19
3.3 Demonstrative Study ..... 19
3.3.1 Powerline Disruption ..... 20
3.3.2 Road Closure ..... 21
3.3.3 Transportation Network Performance ..... 22
3.3.4 Measures for Improving Infrastructure Performance ..... 25

**4. CONCLUSIONS ..... 28**

**REFERENCES ..... 29**

# LIST OF FIGURES

Figure 2.1 Regression plot for American basswood ..... 4
Figure 2.2 Finite element model of a tree ..... 5
Figure 2.3 Flowchart of generating fragility curves of trees ..... 10
Figure 2.4 Stem breakage fragility for three tree species ..... 11
Figure 2.5 Uprooting fragility curves for three tree species ..... 13
Figure 2.6 Windthrow fragility curves for three tree species ..... 15
Figure 3.1 Flowchart of the probabilistic framework to estimate probability of infrastructure disruption ..... 16
Figure 3.2 Schematic diagrams of road blockage induced by fallen trees ..... 17
Figure 3.3 Schematic diagrams of powerline disruption induced by fallen trees ..... 18
Figure 3.4 An abstracted transportation network and powerline system in City of Fort Collins ..... 20
Figure 3.5 Probability of failure of powerline under different wind conditions ..... 21
Figure 3.6 Probability of road closure under different wind conditions ..... 22
Figure 3.7 Probability of disconnection of the OD pair ..... 23
Figure 3.8 The probability mass function of OD travel time ($\alpha$ = 30°, $U$ = 20 m/s) ..... 24
Figure 3.9 The cumulative distribution function of OD travel time (α = 30°) ..... 24
Figure 3.10 Travel time reliability ..... 25
Figure 3.11 Windthrow fragility curves for basswood before and after crown thinning ..... 26
Figure 3.12 Powerline disruption probability and road closure probability before and after crown thinning ..... 26
Figure 3.13 Disconnection probability and travel time reliability before and after crown thinning ..... 27

# LIST OF TABLES

Table 2.1 Regression results ..... 5
Table 2.2 Wind load statistics of different tree species ..... 9
Table 2.3 Mechanical property statistics of different tree species ..... 9

# 1. INTRODUCTION AND LITERATURE REVIEW

## 1.1 Background

Tree failures due to strong winds in forest and urban areas cause extensive direct and indirect economic and environmental losses. Wind damage to managed forests leads to huge loss of timber yield. For example, in 1999, storm Martin in southwest France caused estimated losses of 26.1 million $m^3$ of wood, which is about 3.5 years of harvest in that area (Cucchi et al. 2004). In urban areas, the destruction of trees under extreme winds result in considerably more indirect loss and disruptions to human life and infrastructures than the direct economic loss of fallen trees. Fallen trees due to extreme winds may threaten human safety, damage buried water pipes and buildings, cause overhead powerline outages, or block transportation routes. All these can seriously jeopardize the resilience of an urban community facing various wind hazards, hamper post-hazard evacuation and rescue operations, and delay critical recovery efforts. For instance, the Great Storm in 1987 caused at least 13 deaths in England, most of whom were killed by fallen trees (Mitchell et al. 1989). After hurricane Isabel in 2003, it took 84 days to remove a total amount of 52,865 $m^3$ of tree debris from roads in Bertie County, North Carolina (Laefer and Pradhan 2006). In hurricane Katrina and Rita in 2005, uprooting of trees due to high winds was the main cause of damage to buried water and wastewater pipes in some Louisiana cities (Chisolm and Matthews 2012). It is therefore very important to develop an efficient risk assessment tool to predict and further reduce the disruptions to critical infrastructures caused by fallen trees in future wind events.

Over the last decades, some models have been developed to predict the risk of tree failure under strong winds; these can be categorized as two main types: statistical models and mechanistic models. Statistical models can predict the windthrow probability and identify key factors associated with wind damage (Lavoie et al. 2012). However, these models are unable to provide evidence of actual damage mechanism and are hard to be generalized for other locations and environments. Although mechanistic models need some modeling simplifications and supporting empirical relationships, they can provide a clear understanding of windthrow mechanism by linking the wind events and trees' performance. Several developed mechanistic models have been widely adopted in the research community for forest trees such as HWIND (Peltola et al. 1999), GALES (Gardiner et al. 2000), and FOREOLE (Ancelin et al. 2004), which can predict the critical wind speeds required to break or overturn trees. These models are commonly employed to estimate wind damage to the forest, serving as forest management decision support tools. Compared with forest trees, urban trees tend to have a broader crown, and more and larger branches, indicating larger applied wind loads and likely higher windthrow risk. However, very few research studies have focused on failure modeling of urban trees due to strong winds (Ai et al. 2016; Kocatepe et al. 2018).

Fragility is defined as the probability of exceeding a prescribed limit state for a given measure of hazard intensity, and fragility analysis has been widely conducted for the performance assessment of various structures in seismic and wind hazards. However, tree fragility study under strong winds has not received the attention it deserves. Ciftci et al. (2014) proposed a method to obtain the fragility curves for amenity trees due to windstorms, and a dynamic time history analysis of a detailed finite element tree model was carried out to determine the maximum wind-induced bending moment in the tree stem. However, in their study the fragility analysis was conducted for only two specific trees rather than a number of tree classes for each species, making it inappropriate for the risk assessment covering various uncertainties. Kocatepe et al. (2018) identified four common tree species in Tallahassee, Florida, based on the convolutional neural network (CNN) method and estimated tree fragility curves with the Monte Carlo simulation. However, the mechanistic model for predicting tree failure induced by winds was rather simplified. Moreover, only stem breakage was considered and another type of major failure, uprooting, was not covered in the tree fragility studies as illustrated above.

There have been many research works related to infrastructure disruption due to the interaction between damaged buildings and the infrastructure itself subjected to natural disasters. Road blockages due to fallen debris from collapsed buildings after earthquakes cause reduced traffic capacity and increased travel delay, which significantly affect the post-earthquake emergency response and recovery of other infrastructures. The interaction between transportation networks and buildings damaged by earthquakes has been extensively studied (Goretti and Sarli 2006; Argyroudis et al. 2015; Zanini et al. 2017). In contrast, despite catastrophic consequences to human life and infrastructures resulting from tree failure in past windstorms, research regarding the risk of critical infrastructures caused by tree damage is very limited. Using a GIS-based methodology, Kocatepe et al. (2018) evaluated the accessibility to critical emergency facilities in a transportation network disrupted by tree failure during hurricanes. Laefer and Pradhan (2006) proposed a methodology to identify potentially hazardous trees that may endanger transportation routes by utilizing GIS and airborne laser altimetry data, which have the potential for evacuation route selection. Poulos and Camp (2010, 2011) developed a decision support system for identifying locations where powerlines can be disrupted by vulnerable trees during storms.

## 1.2 Organization of Report

There are two objectives in this study: (1) to develop fragility curves for typical urban tree species under extreme winds, and (2) to probabilistically assess the performance of disrupted overhead powerlines and transportation infrastructures due to fallen trees by employing tree fragility curves. In this study, we first develop allometric equations for three urban tree species to facilitate the development of the mechanistic model and fragility curves. Second, a mechanistic model based on finite element modeling is built with the direct stiffness method by considering wind profile, wind loads, and self-weight of trees. Third, fragility curves of three tree species are generated for both stem-breaking and uprooting limit states through Monte Carlo simulation. Finally, in the small community of Fort Collins, the performance of disrupted critical infrastructures, such as transportation and overhead powerline infrastructures, due to fallen trees is evaluated with the proposed probabilistic method. The proposed tree fragility and performance assessment framework can help people understand the risks of tree failure and the impacts to some critical infrastructures and the community resilience in a specific wind event. Accordingly, the stakeholders can make risk-informed decisions in terms of effective prevention and preparation measures to protect these infrastructures and further improve the resilience of the entire community subjected to wind events.

The report is composed of four chapters: Chapter 1 introduces pertinent background information and literature review results related to the present study. In Chapter 2, the modeling process of traffic safety assessment methodology is introduced. In Chapter 3, numerical demonstration of the new modeling technique is conducted, and the results are discussed. Chapter 4 summarizes the findings from the report.

# 2. FRAGILITY MODEL OF URBAN TREES SUBJECTED TO EXTREME WINDS

## 2.1 Description of Urban Trees

Depending on their species and ages, different trees have different profiles. To characterize a specific tree, there are some commonly used parameters, such as age, tree height, diameter at breast height (DBH), crown height, and crown diameter. Tree allometry is widely used in forest management to establish the quantitative relationship between these parameters, with which some hard-measured parameters can be predicted with an easily measured one. With allometric equations, DBH can be predicted with age and total height. Crown diameter and crown height can be predicted with DBH. In urban forestry, allometric equations can help urban forest managers in selecting species, developing tree removal and replacement plans, and estimating management costs and ecosystem services (Peper et al. 2014). Measured field data are important in the development of reliable allometric equations. U.S. Forest Service Pacific Southwest Research Station measured 14,487 urban street and park trees in 17 U.S. cities, constructed the Urban Tree Database (UTD), and developed 365 sets of allometric equations for 171 distinct tree species (McPherson et al. 2016).

In this study, the measured tree data in Fort Collins from the UTD are used to develop allometric equations for three popular street tree species: American basswood, green ash, and ponderosa pine. Compared with other parameters, tree height is much easier to be measured, and is also a more intuitive input for a mechanistic tree model. In this study, we adopt tree height to estimate DBH, crown height, and crown diameter with the polynomial models developed by McPherson et al. (2016). A linear model is used to fit the data points of three tree species, which have the following form:

$$y_i = a + bx_i + \frac{\varepsilon_i}{\sqrt{w_i}} \tag{1a}$$

where $y_i$ is the measurement of tree $i$, which refers to DBH, crown diameter, and crown height; $a$ and $b$ are constants to be estimated; $x_i$ is the height of tree $i$; $\varepsilon_i$ is the random error for tree $i$ with $\varepsilon_i \sim N(0, \sigma^2)$; $\sigma^2$ is the variance of the random error; $w_i$ is the weight and $w_i = 1/x_i^2$.

Statistical analysis was conducted using MATLAB and the regression plots for American basswood are given in Figure 2.1. Regression results for three tree species are listed in Table 2.1. Note that the adjusted $R^2$ are larger than 84% for DBH, crown diameter, and crown height, indicating good fitting results. With the developed allometric equations, a tree can be defined with tree height, facilitating the following development of fragility curves for different tree classes in terms of tree height.

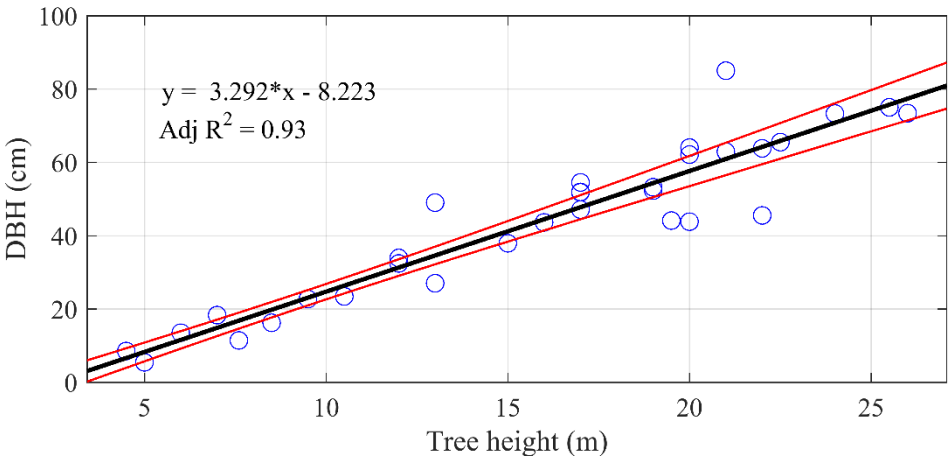


(a) DBH

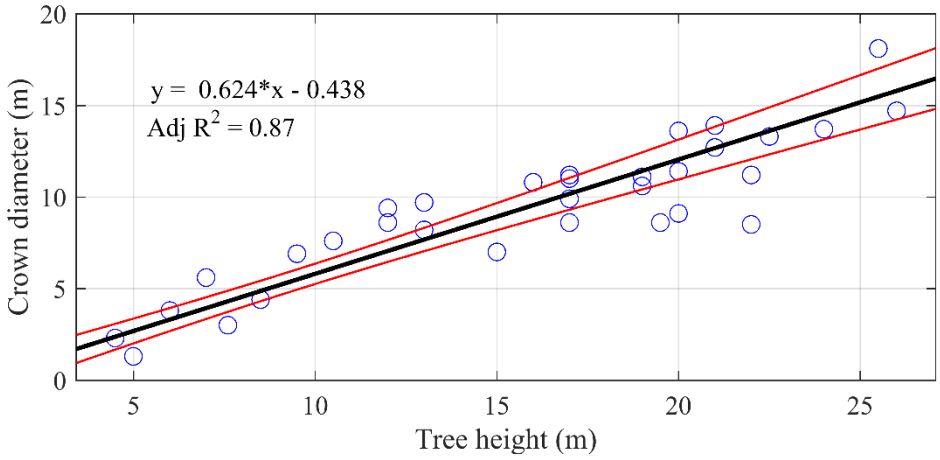


(b) Crown diameter

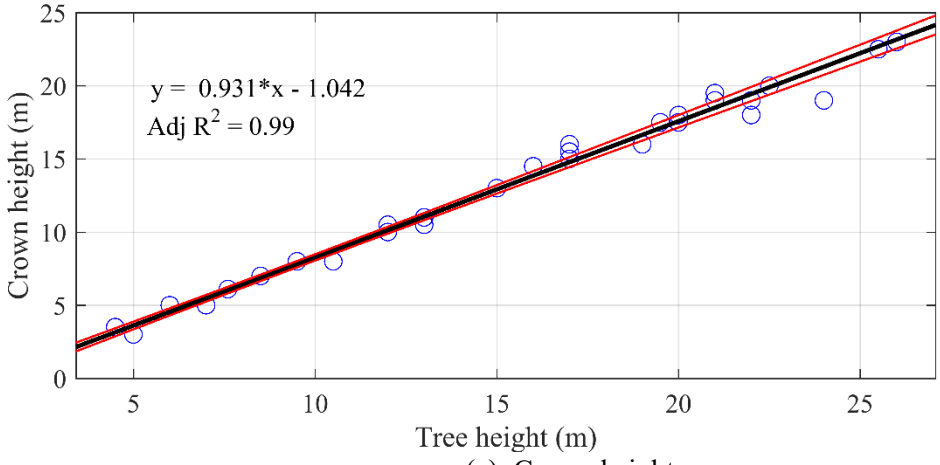


(c) Crown height

**Figure 2.1** Regression plot for American basswood

**Table 2.1** Regression results

| Tree species | DBH | | | Crown diameter | | | Crown height | | |
|---|---|---|---|---|---|---|---|---|---|
| | a | b | Adj $R^2$ | a | b | Adj $R^2$ | a | b | Adj $R^2$ |
| American basswood | 3.292 | -8.223 | 0.93 | 0.624 | -0.438 | 0.87 | 0.931 | -1.042 | 0.99 |
| Green ash | 4.379 | -10.41 | 0.89 | 0.892 | -0.589 | 0.88 | 0.808 | -0.383 | 0.97 |
| Ponderosa pine | 3.74 | -2.195 | 0.84 | 0.673 | 0.388 | 0.86 | 0.815 | 0.252 | 0.94 |

## 2.2 Mechanistic Tree Model

A mechanistic tree model is built with the direct stiffness method, which describes the behavior of a tree under winds and computes the internal forces of the tree structure. With a sufficient number of elements, a tapered tree stem can be discretized into multiple beam elements with an approximate uniform cross section for each element, as shown in Figure 2.2. The properties of the uniform cross sections are defined based on those at the middle point of each element, following typical finite element modeling technique of tapered structures. Based on the applied external forces, element properties, and boundary conditions, the equilibrium equations of the discretized tree system are formulated into a matrix relationship. Then, free nodal displacements, support reactions, and element forces are numerically solved with the tree finite element model (FEM).

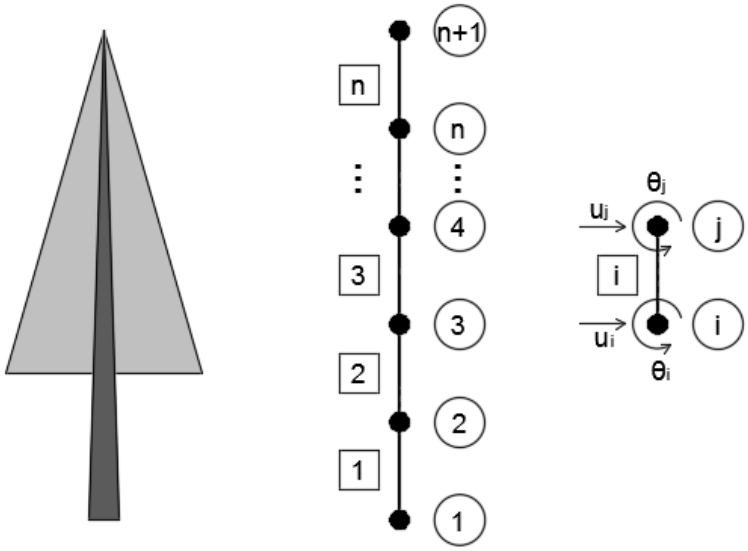


**Figure 2.2** Finite element model of a tree

### 2.2.1 Wind Loads

Although aerodynamic analysis of trees subjected to wind is supposed to generate more accurate results of tree response under winds, it requires tree-profile-specific wind coefficients typically obtained from wind tunnel tests, which are not yet available. In addition, the additional high computational cost of aerodynamic analysis will also cause overwhelming computational burden for the following fragility analysis. Therefore, in this study, only aerostatic analyses of the trees are conducted. The 3-s gust wind speed is used to calculate the wind forces acting on the tree in this study, and the 3-s gust wind profile can be defined in the power-law form (Simiu and Miyata 2006) as expressed in Eq. (1b):

$$V(z) = V(10)\left(\frac{z}{10}\right)^{\alpha} \tag{1b}$$

where $z$ is height (m); $V(z)$ is the 3-s gust wind speed at height $z$ (m/s); $\alpha$ is the ground roughness coefficient, which is taken as 0.143 for suburban terrain and town.

The horizontal wind forces acting on both the stem and crown are considered; these are calculated based on the wind profile, the stem taper equation, and the assumed crown shape. The uniformly distributed drag forces (Unit: N/m) acting on stem element $i$ can be expressed as follows:

$$F_{WS,i} = 0.5\rho_{air}C_{dS}D_{S,i}V_i^2 \tag{2}$$

where $\rho_{air}$ is the air density (kg/m$^3$); $C_{dS}$ is the drag coefficient of the stem; $D_{S,i}$ is the diameter at the mid-height of stem element $i$ (m), which is determined by the stem taper equation $D_S(h)$; $h$ is the tree height (m); and $V_i$ is the 3-s gust wind speed at the mid-height of element $i$ (m/s).

Without specific tree profile data, the unstreamlined crown projection area against the wind is computed by assuming the tree crown has a triangular shape (Peltola et al. 1999). The canopy becomes streamlined as the wind speed increases, leading to a reduction of crown area, which is assumed to be controlled by a streamlining coefficient, $S_t$ (Peltola et al. 1999). The uniform distributed drag forces (Unit: N/m) acting on the crown element $i$ can be given by:

$$F_{WC,i} = 0.5\rho_{air}C_{dC}D_{C,i}S_t(V_{g,i})V_i^2 \tag{3}$$

where $C_{dC}$ is the drag coefficient of the crown; $D_{C,i}$ is the diameter at the mid-height of crown element $i$ (m).

### 2.2.2 Self-weight

Self-weight of a tree contributes to the normal compressive stress in the stem and also brings additional moment due to the P-Delta effects under wind loads, which further increases the axial compressive stress. The total weight of each element is the sum of the weights of the stem and crown. The weight of stem element $i$ is calculated as follows:

$$F_{GS,i} = 0.25\rho_S g L_i \pi D_{S,i}^2 \tag{4}$$

where $\rho_S$ is the stem density (kg/m$^3$); $g$ is the acceleration of gravity (m/s$^2$). Similarly, the weight of crown element $i$ is calculated through Eq. (5):

$$F_{GC,i} = 0.25\rho_C g L_i \pi D_{C,i}^2 \tag{5}$$

where $\rho_C$ is the crown density (kg/m$^3$), which is estimated by assuming a constant ratio between the crown and stem weights.

### 2.2.3 Application of Direct Stiffness Method

To consider the P-Delta effects due to gravity forces, first-order analysis is performed to obtain the axial forces in each element based on the computed stem and crown weights. The geometric stiffness matrix $k_G$ of each element is then calculated based on the obtained axial forces. For a beam element, $k_G$ is only a function of the element's length and the axial force in the element, which can be computed by Eq. (6).

$$k_G = \frac{N}{30L}\begin{bmatrix} 36 & 3L & -36 & 3L \\ 3L & 4L^2 & -3L & -L^2 \\ -36 & -3L & 36 & -3L \\ 3L & -L^2 & -3L & 4L^2 \end{bmatrix} \tag{6}$$

where $N$ is the axial force in a beam element; $L$ is the element length.

By adding the geometric stiffness matrix $k_G$ to the elastic stiffness matrix $k_E$ as defined in Eq. (7), we can obtain the total stiffness matrix $k_E + k_G$ for each element, which will be assembled into the global stiffness matrix $K_E + K_G$. The wind forces acting on each element will be converted to equivalent nodal loads and then assembled into the global nodal load vector $F$.

$$k_E = \frac{EI}{L^3}\begin{bmatrix} 12 & 6L & -12 & 6L \\ 6L & 4L^2 & -6L & 2L^2 \\ -12 & -6L & 12 & -6L \\ 6L & 2L^2 & -6L & 4L^2 \end{bmatrix} \tag{7}$$

where $E$ is the modulus of elasticity; $I$ is the moment of inertia.

Finally, the equations of the global system can be derived as Eq. (8).

$$(K_E + K_G)U = F \tag{8}$$

where $U$ is the global nodal displacement.

By solving Eq. (8), the global nodal displacements can be obtained:

$$\mathrm{U} = (K_E + K_G)^{-1}F \tag{9}$$

With the global nodal displacements, the support reactions and element forces can be calculated. Under the combined effect of bending moment and normal forces, the total compressive stress (Pa) in the outer fibers of stem element $i$ is given as

$$\sigma_i = \frac{M_i}{I_i}\frac{D_{S,i}}{2} + \frac{N_i}{A_i} \tag{10}$$

where $M_i$ is the moment in element $i$; $N_i$ is the axial force; $I_i$ is the moment of inertia; $A_i$ is the area.

## 2.3 Limit State

There are two failure modes for a tree under strong winds: stem breakage and uprooting. Stem breakage occurs when the maximum compressive stress $\sigma_{max}$ in the stem exceeds the stem modulus of rupture $\sigma_R$. The limit state defining the stem breakage of a tree can be expressed as

$$g_b = \sigma_R - \sigma_{max} \tag{11}$$

It is possible that stem breakage only occurs at a small portion of the crown top, e.g., the top tip of the crown, which may not necessarily cause potential infrastructure disruption (e.g., road blockage). Therefore, the stem breakage condition is assessed based on the elements below the mid-crown height to avoid overrepresentation of infrastructure disruption. Once the stem breakage occurs, the breakage ratio, which is defined as the ratio of the length of the broken stem to the total tree height, will be recorded according to the breakage location.

Uprooting occurs when the critical turning moment $M_o^{cri}$ provided by the root-soil plate anchorage is exceeded by the base turning moment $M_{max}$ produced by wind. The critical overturning moment $M_o^{cri}$ can be determined by tree pulling experiments and is strongly related to stem weight $W_s$ (Gardiner et al. 2000). The relationship can be expressed as follows:

$$M_o^{cri} = C_{reg} W_s \tag{12}$$

where $C_{reg}$ is the regression constant, which is dependent on species and soil conditions ($NmKg^{-1}$). Therefore, the limit state of uprooting of a tree can be expressed as

$$g_u = M_o^{cri} - M_{max} = C_{reg} W_s - M_{max} \tag{13}$$

## 2.4 Statistics of Wind Loads and Mechanical Properties of Trees

Uncertainties exist in wind loads and mechanical tree properties, which need to be modeled probabilistically in fragility analyses. The statistics of the wind load-related parameters for different tree species are summarized in Table 2.2. Note that the crown characteristics of deciduous trees (e.g., American basswood and green ash) change between seasons. For example, the drag coefficient and weight of the crowns of deciduous trees in summer are larger than those in winter, making them more susceptible to windthrow. The crown characteristics of trees in summer are used in this study to be conservative. The drag coefficients of tree crown and stem and the streamlining coefficient are assumed to follow normal distributions. For the three tree species studied here, the drag coefficient of the stems with cylinder cross sections is assumed to have a mean value of 1.0 and coefficient of variation (COV) of 0.1. According to Horacek (2003), the mean values of the drag coefficients of crowns for American basswood, green ash, and ponderosa pine are 0.25, 0.25, and 0.3, respectively. The COVs for the three species are assumed to be 0.2. The mean values of the streamlining coefficients of three tree species are 0.4 following the study by Peltola et al. (1999), and the COV is assumed to be 0.2. Triangle, which is used to calculate the wind loads acting on the crown, has proven to be an appropriate shape to model the reconfigured frontal crown shape under wind. Deterministic stem taper equations for the three tree species developed by Westfall and Scott (2010) are used in this study.

**Table 2.2** Wind load statistics of different tree species

| Variables | Mean | | | COV | CDF | Source |
|---|---|---|---|---|---|---|
| | AB | GA | PP | | | |
| Drag coefficient of crown | 0.25 | 0.25 | 0.30 | 0.2 | Normal | Horacek (2003) |
| Drag coefficient of stem | | 1 | | 0.1 | Normal | Anderson Jr (2010) |
| Streamlining coefficient | | 0.4 | | 0.2 | Normal | Peltola et al. (1999) |
| Crown shape | | Triangle | | | Deterministic | |
| Stem taper equation | | / | | | Deterministic | Westfall and Scott (2010) |

Note: AB, GA, and PP represent American basswood, green ash, and ponderosa pine, respectively

Table 2.3 summarizes the mechanical property statistics for different tree species. Mechanical properties of trees are species-dependent and are usually obtained from extensive sampling and analysis procedures. In this study, without more statistical information, all these parameters are assumed to follow normal distributions. The statistics of the stem density, modulus of rupture, and modulus of elasticity for green wood of three tree species can be found in the Wood Handbook (Ross 2010). The mean value and COV of the crown to stem weight ratio, which can determine the crown density, are taken from the previous study by Peltola et al. (1999). The regression constant of ponderosa pine is obtained from the pulling experiments (Gardiner et al. 2000), but no such data have been found for American basswood and green ash in previous studies. Dupuy et al. (2005) found that the tap root is twice as resistant as the plate-like root of hardwood trees, such as American basswood and green ash. Therefore, in this study, the regression constants of American basswood and green ash are assumed to be half that of ponderosa pine.

**Table 2.3** Mechanical property statistics of different tree species

| Variables | Mean | | | COV | CDF | Source |
|---|---|---|---|---|---|---|
| | AB | GA | PP | | | |
| Stem density (kg/m$^3$) | 320 | 530 | 380 | 0.1 | Normal | Ross (2010) |
| Modulus of rupture (MPa) | 34 | 66 | 35 | 0.16 | Normal | |
| Modulus of elasticity (MPa) | 7200 | 9700 | 6900 | 0.22 | Normal | |
| Crown to stem weight ratio | 0.4 | 0.3 | 0.4 | 0.25 | Normal | Peltola et al. (1999) |
| Regression constant (NmKg$^{-1}$) | 67 | 67 | 134 | 0.2 | Normal | Gardiner et al. (2000)<br>Dupuy et al. (2005) |

## 2.5 Development of Fragility Curves

Fragility function represents the probability of exceeding a limit state under a given hazard intensity:

$$Fragility = \Phi\left(\frac{\ln(im/m_R)}{\xi_R}\right) = P(EDP > LS|IM = im) \tag{14}$$

where $\Phi(\cdot)$ is the standard normal distribution function; $P(\cdot)$ is the probability function; $IM$ is hazard intensity measure; $im$ is a particular value of $IM$; $EDP$ is the engineering demand parameter; $LS$ is the limit state value associated with the $EDP$ being considered; $m_R$ is the median capacity; $\xi_R$ is the logarithmic standard deviation.

For the two limit states defined in Eqs. (11) and (13), $EDP$ refers to the maximum compressive stress of the stem $\sigma_{max}$ and the stem modulus of rupture $\sigma_R$ for the stem breakage limit state; and base bending moment $M_{max}$ and critical overturning moment $M_0^{cri}$ for the uprooting limit state, respectively. A 3-s gust wind speed at the height of 10 m is chosen as $IM$.

To avoid performing fragility analysis for every single tree, which will require cost-prohibitive computational and modeling efforts, mean fragility is estimated for tree classes grouped according to tree heights. Trees with heights ranging from 7 m to 29 m are divided into 11 classes and each class covers a height range of 2 m. Tree heights within each class follow uniform distributions. Other tree profile parameters such as DBH, crown height, and crown diameter are determined with the developed allometric equations. For each tree class of a tree species, Monte Carlo simulation is used to generate 10,000 random samples, including data related to mechanical properties, wind load, and tree profile according to their statistics in Table 2 and 3. Each sample builds a tree mechanistic model under a given wind condition, and then the simulation results are checked against the two limit state functions, respectively. With the simulation results from all generated samples, fragility curves for stem breakage and uprooting can be obtained. Figure 2.3 shows the flowchart of developing the fragility curves of the trees subjected to winds.

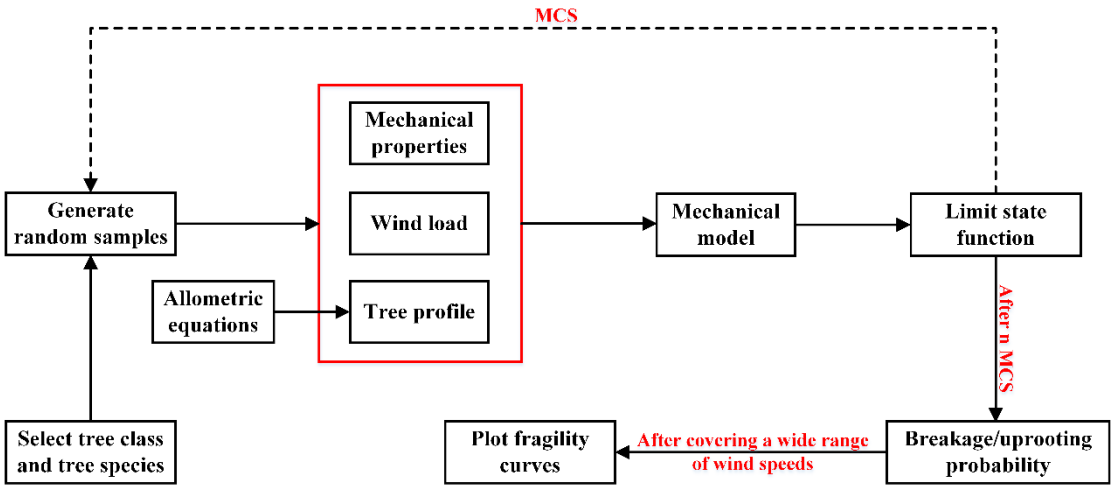


**Figure 2.3** Flowchart of generating fragility curves of trees

Figure 2.4 illustrates the stem breakage fragility for the three tree species. Five selected tree classes with different tree heights, namely 9 - 11 m, 13 - 15 m, 17 - 19 m, 21 - 23 m, and 25 - 27 m, are considered. The calculated fragility results, which are represented by the black circles in Figure 2.4, are compared with lognormal cumulative distributions obtained by best-fit analysis. It is seen that lognormal distribution can capture the general trend of fragilities obtained by the Monte Carlo simulation. As might be expected, the vulnerability of stem breakage increases with the increase of tree heights for all three tree species. Generally, green ash is less vulnerable to stem breakage than the other two tree species due to its higher modulus of rupture.

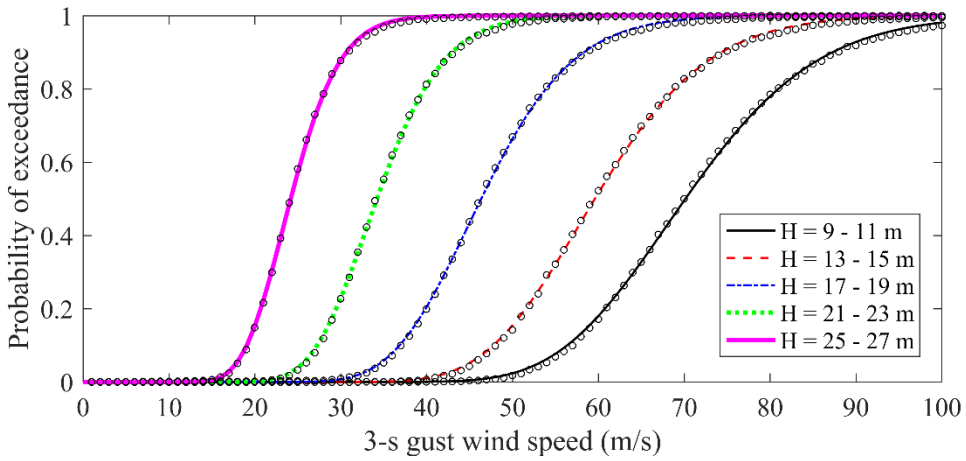


(a) American basswood

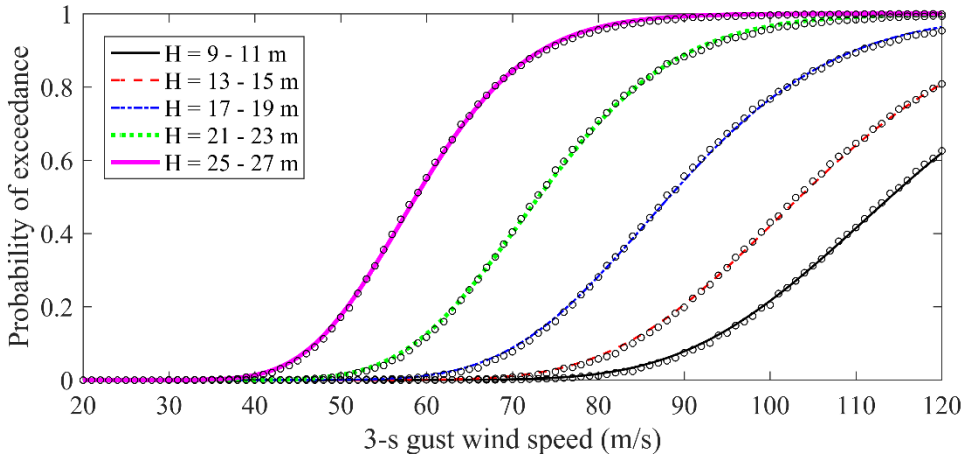


(b) Green ash

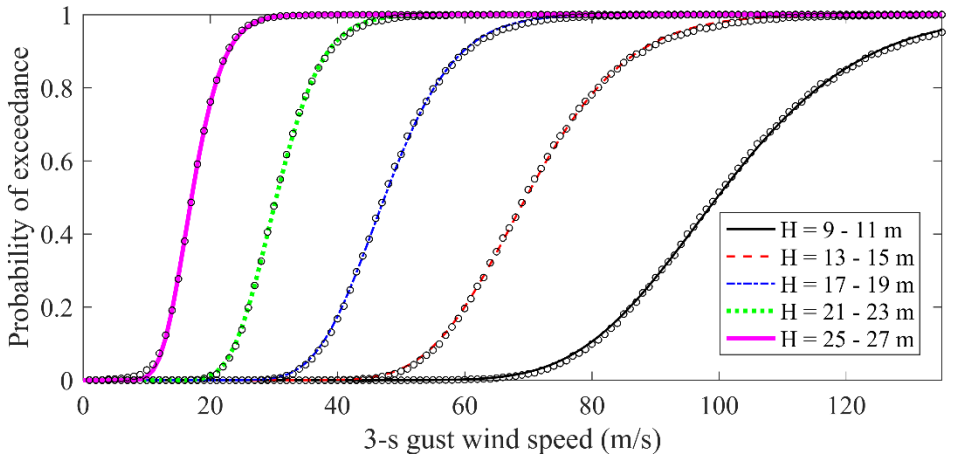


(c) Ponderosa pine

**Figure 2.4** Stem breakage fragility for three tree species

Figure 2.5 presents uprooting fragility curves for three tree species. Unlike American basswood and ponderosa pine, uprooting fragility curves of green ash show decreasing vulnerability with the increase of tree heights. According to the uprooting limit state defined in Eq. (13), stem weight contributes to both the demand and capacity. It is likely that the contribution to the capacity outweighs that to the demand when the tree height for green ash increases. Ponderosa pine is less vulnerable than the other two tree species due to its higher resistive moment. Meanwhile, when the tree height is larger than 17 m, the fragility curves of different classes are very close, indicating that the effect of tree height on the uprooting fragility is insignificant.

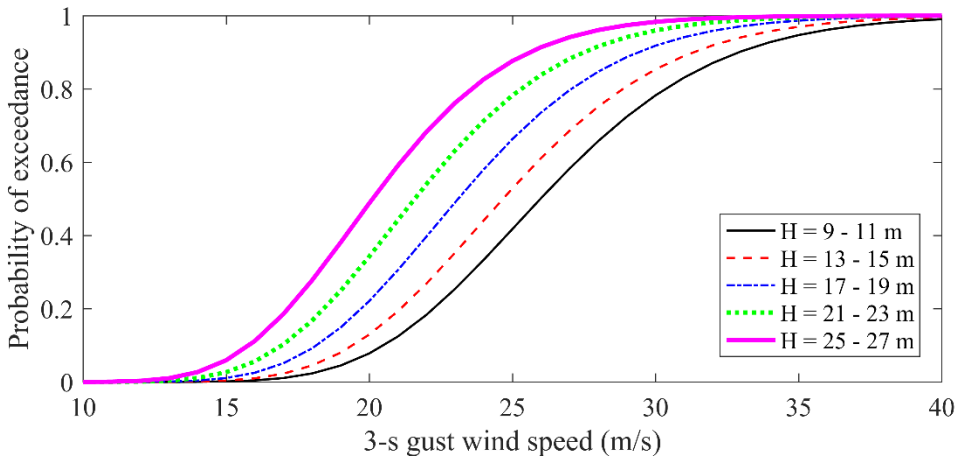


(a) American basswood

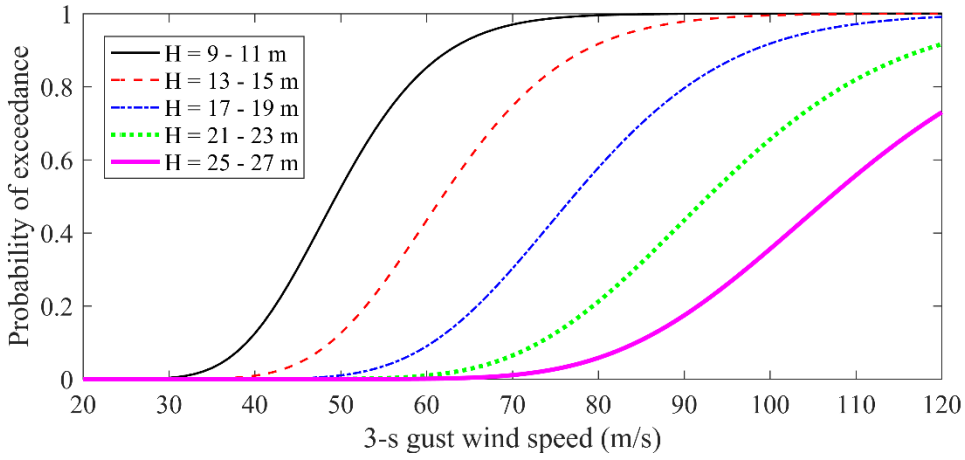


(b) Green ash

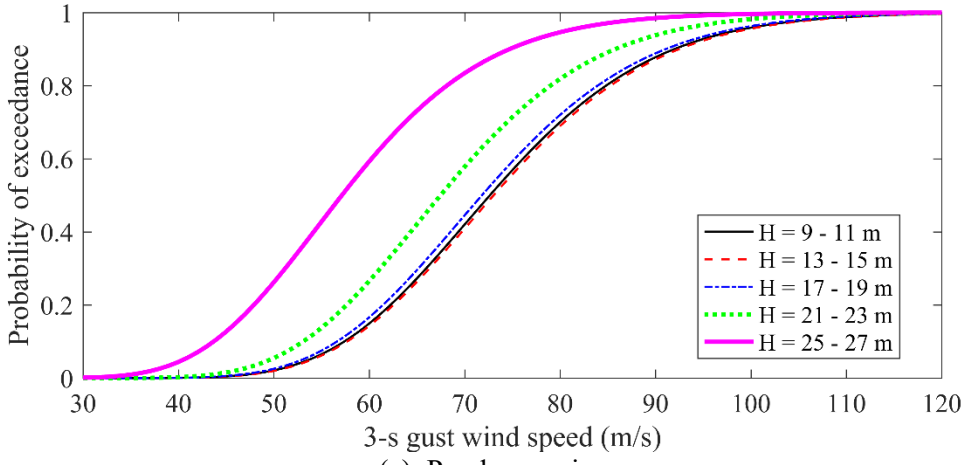


(c) Ponderosa pine

**Figure 2.5** Uprooting fragility curves for three tree species

Windthrow includes stem breakage and uprooting. If at least one of the two failure modes occur, windthrow is deemed to occur. The windthrow fragility of a tree can be derived by assembling fragility of two failure modes. Figure 2.6 shows the windthrow fragility curves for the three tree species. It is found that windthrow of American basswood is dominated by uprooting failure, while windthrow of ponderosa pine is mainly dominated by the stem breakage failure except for those trees with heights below 11 m. The windthrow probabilities of American basswood and ponderosa pine increase with the increase of tree height. For green ash, the fragility curves of different tree classes do not exhibit a clear trend with tree heights. By comparing Figure (2.6b) with Figures (2.4b) and (2.5b), it is found that uprooting dominates when tree height ranges from 9 to 19 m, whereas stem breakage dominates when tree height ranges from 21 to 27m. Generally, the results show that American basswood is most vulnerable to wind, while green ash is least vulnerable to wind among the three tree species. This is consistent with previous research findings regarding the wind resistance classification for different tree species by Duryea and Kampf (2007). American basswood and ponderosa pine are considered to have the least and medium-low wind resistance, respectively, while green ash has a medium-high wind resistance.

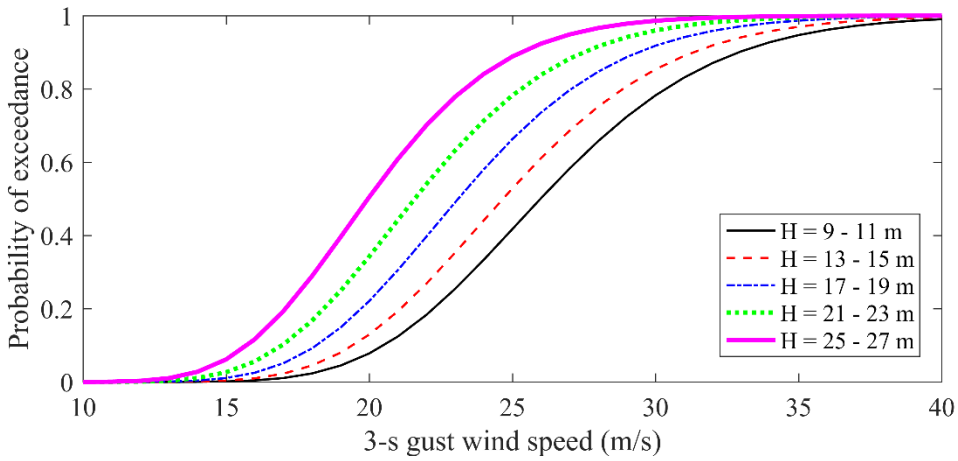


(a) American basswood

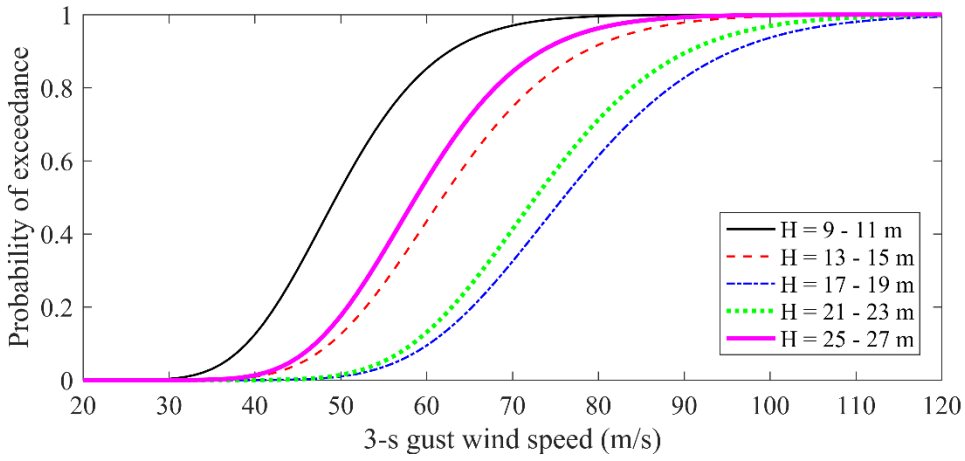


(b) Green ash

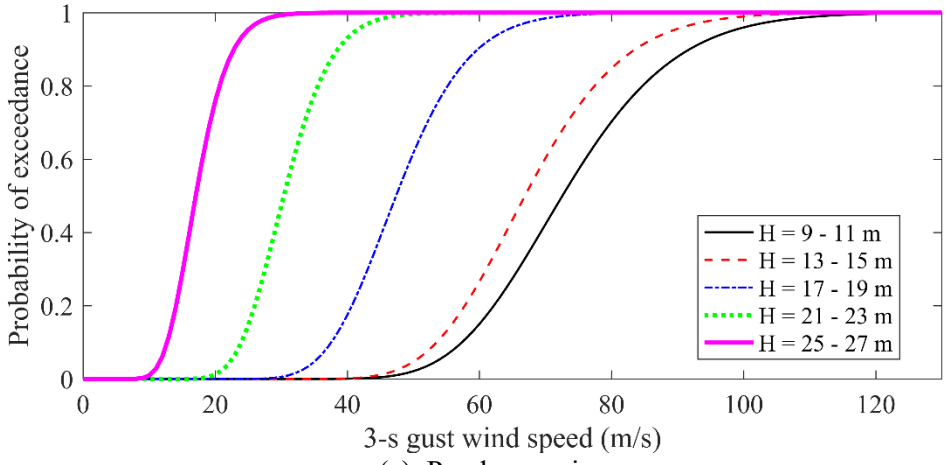


(c) Ponderosa pine

**Figure 2.6** Windthrow fragility curves for three tree species

# 3. PROBABILISTIC METHDOLOGY OF MODELING DISRUPTED INFRASTRUCTURE DUE TO FALLEN TREES

## 3.1 Probabilistic Model of Infrastructure Disruption

The tree fragility curves developed in the previous section can be used to study the disruption of various infrastructure systems (e.g., transportation system, electrical transmission system, water pipe systems, and building system) in urban areas subjected to extreme winds. A probabilistic framework is proposed to estimate the probability of infrastructure disruption due to downed trees. The flowchart of the proposed framework is shown in Figure 3.1. Under a certain wind condition, the probability of breakage/uprooting of a tree adjacent to an infrastructure can be developed based on the windthrow fragility curves of trees. Note that the windthrow mode of a tree under a given wind speed is determined by the larger one between the probabilities of stem breakage and uprooting. If the probability of stem breakage is higher than that of uprooting, stem breakage will occur first; otherwise, uprooting will occur before breakage. Based on the damage mode of the tree, the infrastructure disruption status due to the fallen tree is determined accordingly based on some predefined criteria. After the probabilities of windthrow of all trees along the infrastructure and the corresponding disruption scenarios of the infrastructure under a given wind condition are obtained, Monte Carlo simulations are used to generate many possible disrupted infrastructure scenarios by considering possible windthrow risks of all the trees. Finally, the probability of infrastructure disruption can be obtained according to the Monte Carlo simulation results.

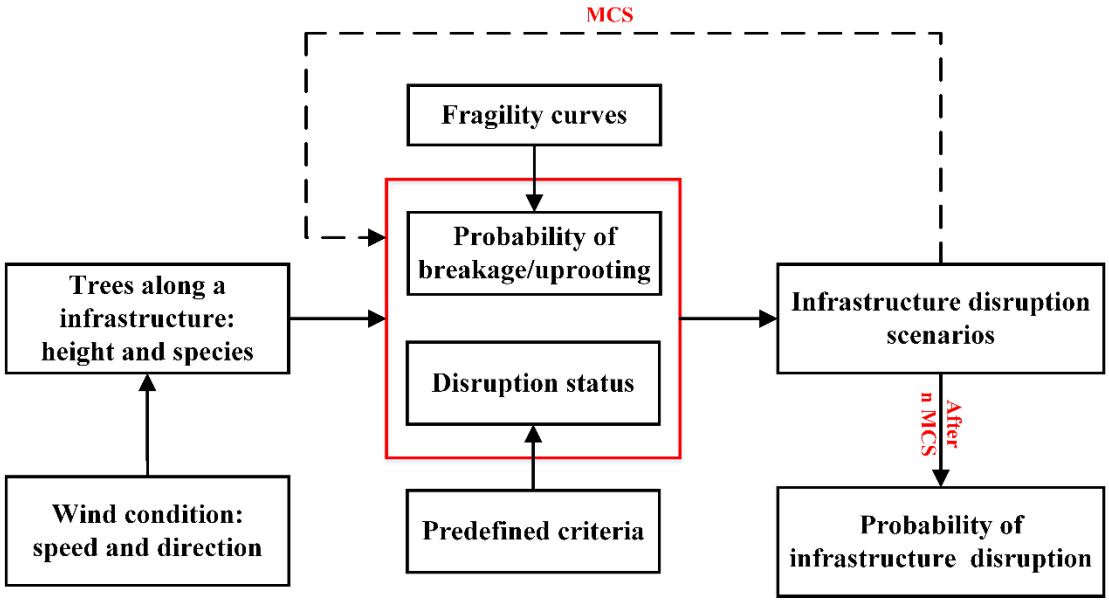


**Figure 3.1** Flowchart of the probabilistic framework to estimate probability of infrastructure disruption

Road blockage and overhead powerline failure induced by fallen trees are demonstrated in detail with the proposed framework, and the corresponding schematic diagrams are shown in Figures 8 and 9. As shown in Figure 3.2, assuming 2.5 m is the minimum open width across the road to enable typical vehicles to pass, a road is deemed being fully blocked by an uprooted or broken tree provided at least one of Eqs. (15) and (16) is satisfied:

$$\text{Road blockage by an uprooted tree: } Hsin(\theta) > D + L - 2.5 \tag{15}$$

$$\text{Road blockage by a broken tree: } H_b sin(\theta) > D + L - 2.5 \tag{16}$$

where $H$ is the tree height (m); $H_b$ is the length of the broken part of the tree (m), which can be obtained from the mechanical model; $\theta$ is the angle between the wind direction and the road direction (°); $D$ is the distance between the tree and the road (m); $L$ is the road width (m).

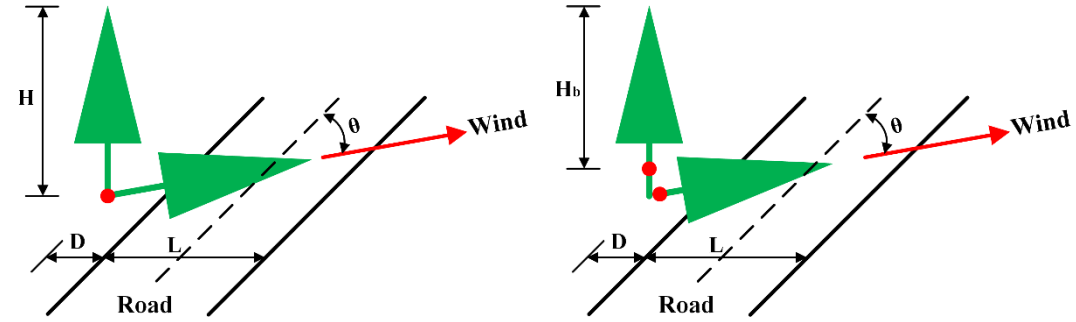


(a) Uprooting (b) Breakage

**Figure 3.2** Schematic diagrams of road blockage induced by fallen trees

As shown in Figure 3.3, if Eq. (17) or Eq. (18) is satisfied, a powerline failure will occur due to the disruption caused by an uprooted or broken tree.

$$\text{Powerline failure by an uprooted tree: } H > H' = \sqrt{h^2 + d'} \tag{17}$$

$$\text{Powerline failure by a broken tree: } H_b > H' = \sqrt{h'^2 + d'} \tag{18}$$

where $h$ is the height of the powerline (m); $d' = d/sin(\theta)$, $d$ is the distance between the tree and the powerline (m); $h' = h - (H - H_b)$.

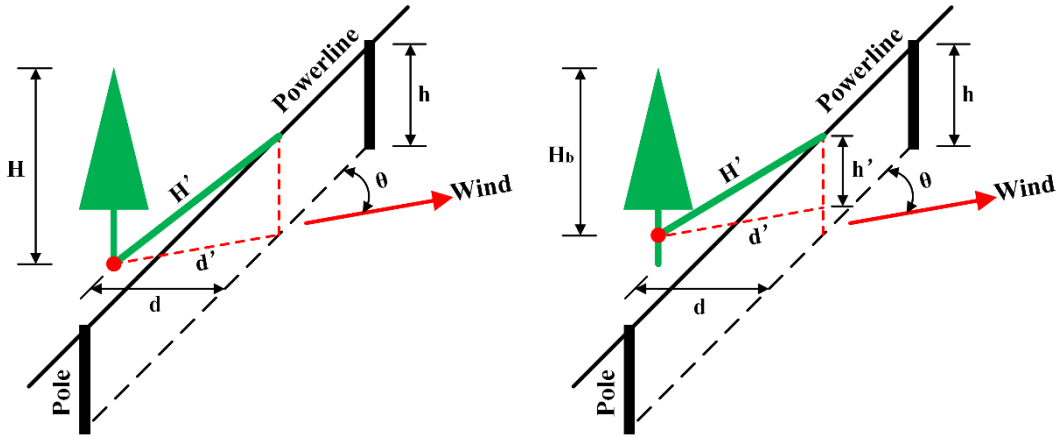


(a) Uprooting (b) Breakage

**Figure 3.3** Schematic diagrams of powerline disruption induced by fallen trees

## 3.2 Transportation Network Analysis in Emergency Response Stage

During and after an extreme wind event, first responders, rescue teams, and emergency vehicles often need to be dispatched to the impacted area through accessible (unblocked) routes as soon as possible. People are interested in knowing not only whether a specific OD pair is connected, but also whether emergency vehicles can arrive at the destination within the expected time frame. Therefore, it is crucial to predict both the connectivity and travel time reliability of potentially disrupted transportation systems due to fallen trees during and following a major windstorm. Such information, which is very different from that in normal conditions and provided by popular map navigation services, will be very helpful for emergency responders and general passengers to identify the optimal travel routes and predict actual travel time following an extreme wind event. The matrix-based system reliability (MSR) method proposed by Kang et al. (2008) is found to be a convenient and efficient tool to compute the connectivity reliability and other quantitative performance measures (e.g., network flow capacity) of a complex system, which will be adopted in the following study.

### 3.2.1 Connectivity Analysis

For the MSR method, the sample space of component events with $d_i$ distinct states, $i = 1, \dots, n$, is divided into $m = \prod_{i=1}^{n} d_i$ mutually exclusive and collectively exhaustive (MECE) events. The probability of a general system event can be obtained with the following formulation:

$$P(E_{sys}) = P_{sys} = \mathbf{c}^{\mathbf{T}}\mathbf{P} \tag{19}$$

where $E_{sys}$ is a general system event; $P_{sys}$ is the probability of the system event; $\mathbf{c}$ is the event vector whose element is 1 if its corresponding MECE event is included in $E_{sys}$, and 0 otherwise; $\mathbf{P}$ is the probability vector that contains the probabilities of all the MECE events. In this study, each component in the infrastructure system (e.g., powerline, road link) has two states due to fallen trees, disrupted and undisrupted, so there will be a total of $2^n$ MECE events. Since the disruption probability of each component of the infrastructure system can be calculated with the probabilistic framework in Section 3.1, the probability vector $\mathbf{P}$ can be easily constructed with simple matrix operations. Then the event vector $\mathbf{c}$ can also be identified separately. Finally, the disconnection probability between two areas can be computed by Eq. (19) with the identified $\mathbf{c}$ and $\mathbf{P}$ vectors. Full details of MSR methods can be found in the reference section (Kang et al. 2008).

### 3.2.2 Travel Time Reliability Analysis

For a specific wind scenario, we perform shortest path analysis for each of the $m$ disruption cases and find the shortest time for an OD pair. For each of the distinct values obtained from the shortest path analysis, $t$, the probability mass function (PMF) and cumulative distribution function (CDF) of the shortest time $T$ for an OD pair can be expressed by Eqs. (20) and (21), respectively.

$$P_T(t) = P(T = t) = \sum_{i:t_i=t}^{m} p_i \tag{20}$$

$$F_T(t) = P(T \leq t) = \sum_{i:t_i \leq t}^{m} p_i \tag{21}$$

where $t_i$ is the shortest OD time for the $i$th disruption case, $p_i$ is the $i$th element in the probability vector **P**. Since it is now focused on an emergency response stage shortly following a windstorm when the traffic demands on the roads are very low, free flow travel time for each passable link is used in the shortest path analysis. For the convenience of presenting the results, a large travel time value, which is 10 times the free flow time on the link, is assigned to a blocked link in the shortest path analysis. Thus, a large OD time instead of an infinite value will be obtained for a disconnected case. Once the CDF is determined, the travel time reliability, $R$, which is the probability that the OD time does not exceed an acceptable threshold level $tt$, can be obtained as

$$R(T \leq tt) = F_T(tt) \tag{22}$$

## 3.3 Demonstrative Study

Downslope windstorms usually occur several times each year along Colorado's Front Range. Winds of 30 to 50 m/s are commonly observed. One severe downslope windstorm event occurred on July 3, 1993, in Fort Collins when wind gusts reached 40 m/s, causing extensive tree and roof damage (Cotton et al. 1995). Given the potential risk due to windthrow on the infrastructures and the availability of data, Fort Collins in Colorado is selected as the demonstrative area in this study. The proposed probabilistic framework, which considers the developed fragility curves of urban trees, is demonstrated through an application to a portion of the transportation network and powerline system in Fort Collins (Figure 3.4). The transportation network consists of 9 nodes (solid circles) and 24 links (solid lines). A residential area (dashed circle with a letter "R") is located close to node 7, and there is a hospital (dashed circle with a letter "H") near node 3. The residential area and the hospital are connected with nearby nodes by subjunctive links (dashed lines), which are assumed to be unaffected by fallen trees due to the lack of large roadside trees along these secondary roads. In addition, there is an overhead powerline system between node 4 and node 6, which consists of two parts: P1 and P2. P1 is located along link 5, and P2 is located along link 8.

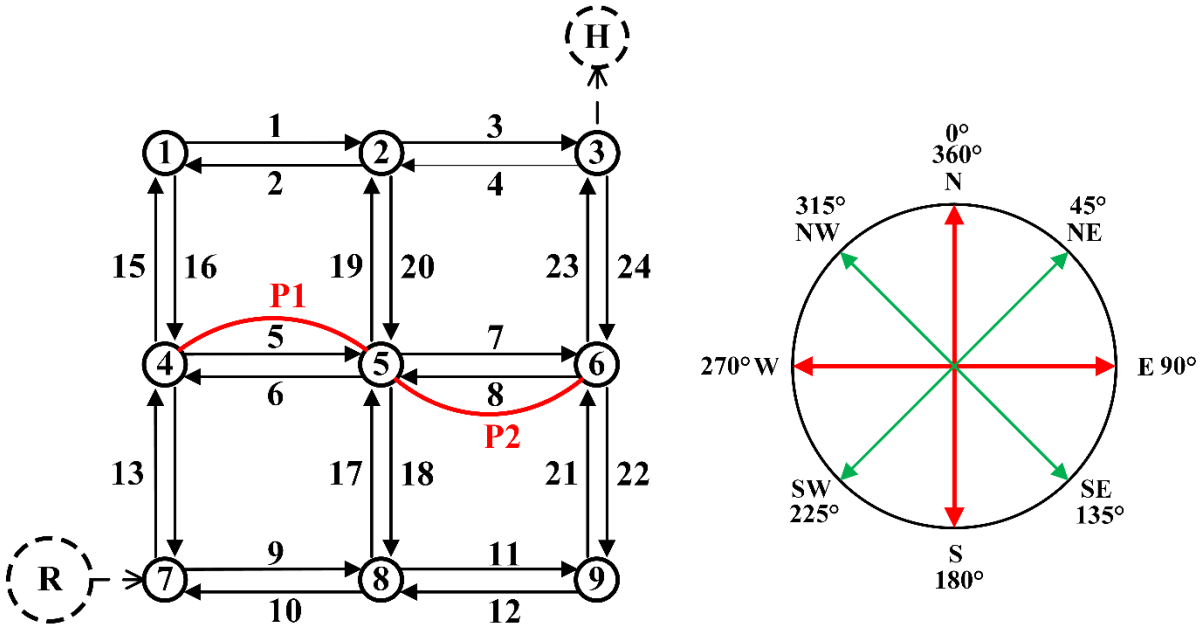


**Figure 3.4** An abstracted transportation network and powerline system in City of Fort Collins

Three popular tree species in Fort Collins are considered in this demonstration. Data from these trees, primarily heights and positions, along the links of the transportation network are collected based on Google Earth. There are 418 trees in this network selected from Fort Collins, with the heights ranging from 8 m to 28 m, and the height of the powerline is found to be 12m.

### 3.3.1 Powerline Disruption

The disruptions (failures) of the overhead powerline system under different wind conditions are investigated. For the overhead powerline system with two parts (P1 and P2), as shown in Figure 10, disruptions will occur if at least one part is hit by at least one fallen tree. Following the proposed framework in Section 3.1, the failure probability of the powerline system under different wind conditions are obtained and plotted in Figure 2.5. Three unfavorable wind directions, $\alpha$ = 180°, 240°, and 360°, are investigated considering that the powerline system is along the EW direction. As expected, the failure probability increases with the wind speed increase. It is also found that south winds ($\alpha$ = 180°) are the most unfavorable events to the powerline system while north winds ($\alpha$ = 360°) are the least. Therefore, south winds control the powerline performance, and this is because the trees along powerline P2 are more vulnerable to winds than those along powerline P1. To reduce the failure risk of the powerline system during an extreme event in a community, it is advised that the city should pay more attention to vulnerable trees along powerline P2.

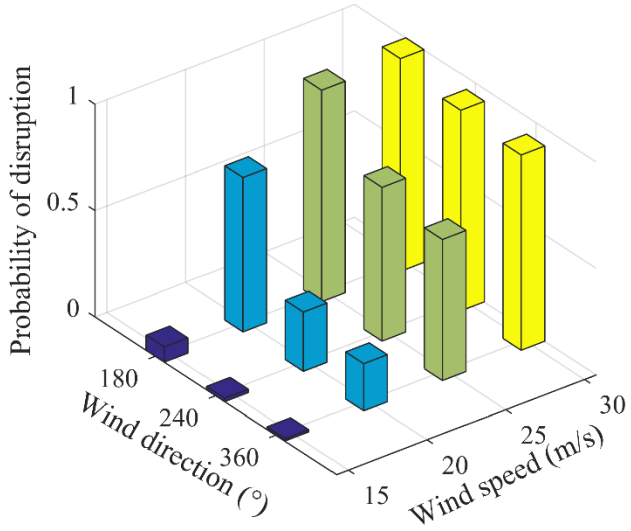


**Figure 3.5** Probability of failure of powerline under different wind conditions

### 3.3.2 Road Closure

Compared with the powerline system, the transportation system is more complicated given a much higher number of roads and different road orientations. Following the proposed framework in Section 3.1, the road closure probability of some selected links is obtained and plotted in Figure 3.6. First, the road closure probability of four links under winds at different speeds but in the same direction ($\alpha = 45°$) is shown in Figure 3.6 (a). As shown in Figure 3.6 (a), the road closure probability increases with the increase of wind speeds for those links. Depending on the species, size, and distribution of adjacent trees, some links are more vulnerable to winds than others, while some links have a very low probability of being blocked. For example, Figure 3.6 (a) shows that Link 7 and 20 have higher closure probability than Link 9 and 22 under the same wind direction and speed. Then, road closure probability of the four links under winds at different directions but the same speed ($U$ = 20 m/s) is shown in Figure 3.6 (b), which shows that the closure probability of links is sensitive to wind direction. As shown in Figure 3.6 (b), for a specific link, closure probability varies with different wind directions. We further find that the road closure probability is influenced by the angle between the wind direction and the link orientation. When the wind direction is perpendicular/parallel to the link orientation, the road closure probability is high/low, respectively, because a fallen tree will cover a large/small road width in this situation. For example, as shown in Figure 3.6 (b), closure probability of Link 6 and 8 in the EW direction is zero under west winds ($\alpha$ = 270°) but is the highest under south winds ($\alpha$ = 180°) among the four directions. Similarly, the closure probabilities of Link 13 and 21 in the NS direction under south winds ($\alpha$ = 180°) are zero but become the highest under west winds ($\alpha$ = 270°) among all four directions. Therefore, it is recommended that the city should pay more attention to vulnerable trees along links that are nearly perpendicular to the prevailing wind directions in windy seasons, including applying some preventive measures.

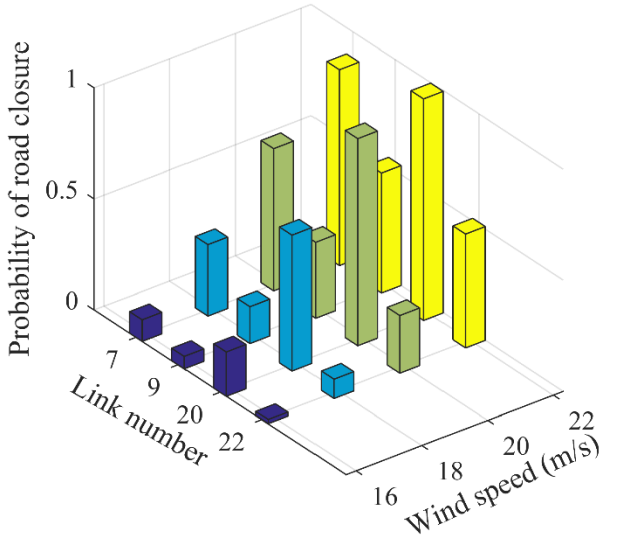


(a) Different wind speeds

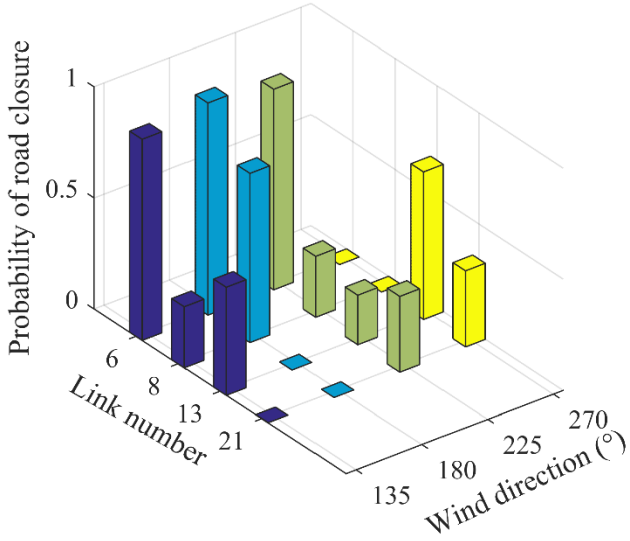


(b) Different wind directions

**Figure 3.6** Probability of road closure under different wind conditions

### 3.3.3 Transportation Network Performance

Of interest for decision-makers is to know the disconnection probability and travel time reliability between the studied residential area and some specific critical infrastructures in the transportation network, such as the hospital, during an impending wind event. The MSR method introduced in Section 3.2.1 is employed to conduct a connectivity analysis of the prototype traffic network for demonstration. After the event vector and probability vector of disconnection between the studied residential area and the hospital are all identified, the disconnection probability of the specific OD pair can be obtained through Eq. (19). The probabilities of disconnections between the residential area and the hospital under different wind conditions are plotted in Figure 3.7.

According to the simulation results, disconnections occur between the OD pair (i.e., the residential area and hospital) under wind directions ranging from -60° (300°) to 45°, mainly around the north direction (Figure 3.7). Additionally, Figure 3.7 shows that north winds cause higher disconnection probability than other winds. This indicates that the trees along the links that are easier to be impacted by north winds ($\alpha$ = 360°), such as Link 1, 3, 5, 7, 9 and 11, may pose higher risks of blocking these links and disconnecting the residential area and the hospital than the other trees. With this information, decision-makers may apply some preventive measures before wind hazards, such as identifying the critical and vulnerable trees, which can be strengthened or trimmed, to reduce the windthrow risk and in turn disconnection probability of the traffic network following the wind event. Meanwhile, they may plan some optimal routes by avoiding those vulnerable links for post-event emergency response, such as police, fire, medical service, and emergency repair.

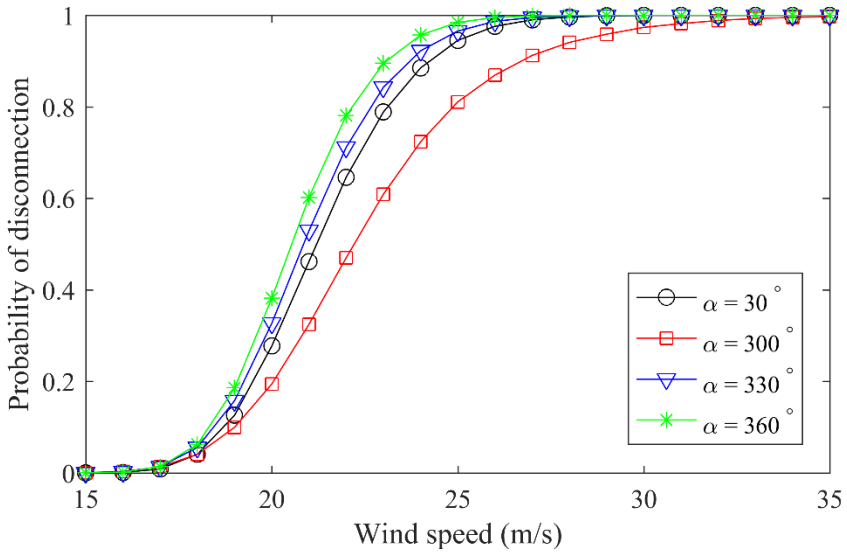


**Figure 3.7** Probability of disconnection of the OD pair

Compared with connectivity, travel time reliability, i.e., the probability that a trip between a given OD pair can be successfully made within a specified time interval, can provide more useful information for the travelers. We then conduct the travel time reliability analysis for the OD pair between the residential area and the hospital with the MSR method introduced in Section 3.2.2.

First, the PMF of the OD travel time under winds with direction $\alpha$ = 30° and speed $U$ = 20 m/s is obtained with Eq. (20) and shown in Figure 3.8. It is found that the minimum travel time is equal to the shortest OD travel time under normal conditions $tt_0$ = 6.03 min, and the corresponding PMF value is 0.435. This indicates there is a 43.5% chance that the shortest OD path between the residential area and the hospital will not be disrupted in this wind event. Note that very large travel time values ($t \geq$ 19.53 min) in Figure 3.8 indicate that all paths between the residential area and the hospital are blocked since we assume a large, instead of infinity, travel time value for blocked links. When the OD travel time is between 6.03 and 19.53 minutes, a detour has been taken because one or more links on the shortest path are blocked.

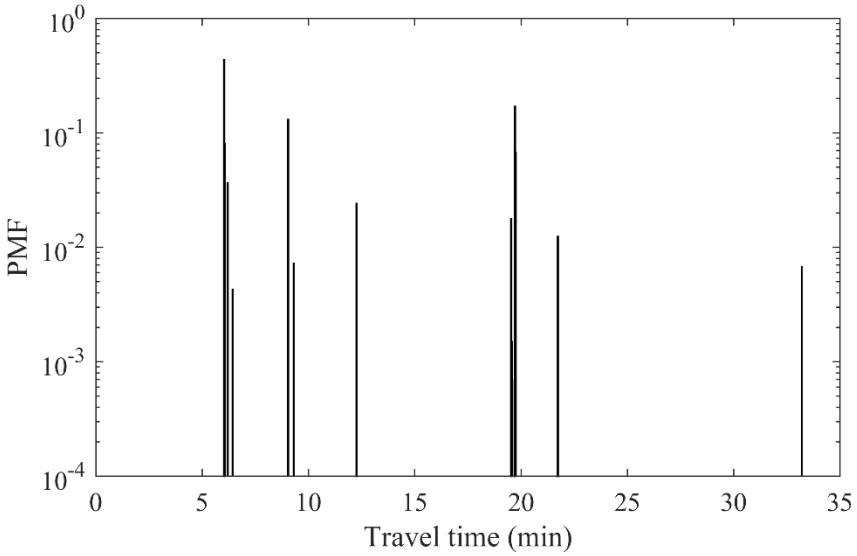


**Figure 3.8** The probability mass function of OD travel time ($\boldsymbol{\alpha}$ = 30°, $\boldsymbol{U}$ = 20 m/s)

Second, the CDFs of the OD travel time under winds with direction $\alpha$ = 30° and speed $U$ = 18, 20 and 22 m/s are obtained with Eq. (21) and shown in Figure 3.9. The figure shows that the CDF, i.e., the probability that the OD travel time does not exceed a given threshold value, decreases significantly as the wind speed increases. For instance, for the three wind speeds $U$ = 18, 20, and 22 m/s, the probabilities that the OD travel time does not exceed 10 minutes (vertical line), are 0.955, 0.699, and 0.324, respectively. Meanwhile, the optimal path during a specific wind event, on which the total travel time does not exceed a given time, can be identified by finding the path with short OD travel time and high probability of OD travel time (PMF) based on the derived travel time distribution. It is found that the optimal path under a given time of 10 minutes for the three wind scenarios (i.e., $\alpha$ = 30° and $U$ = 18, 20, and 22 m/s) are the same: Link 9 → Link 11 → Link 21 → Link 23, which is also the optimal path under normal conditions. Note that the optimal path is sensitive to wind directions and varies with different wind conditions.

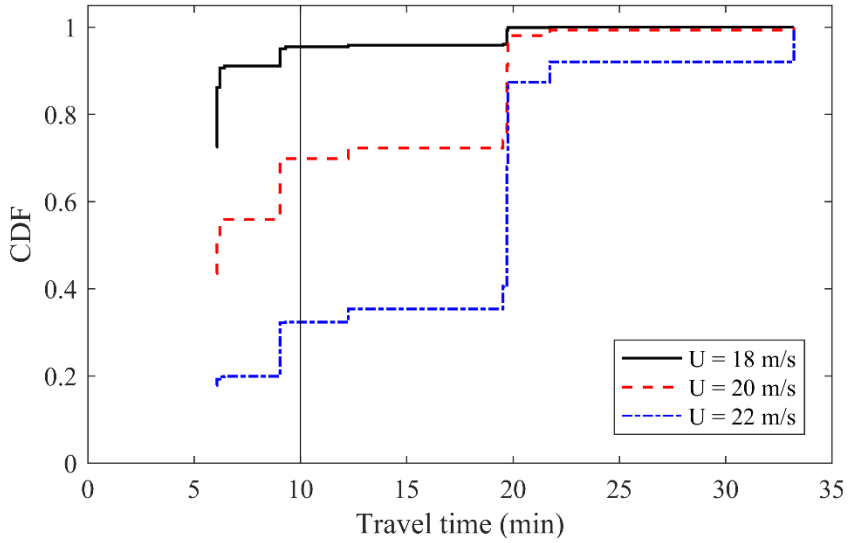


**Figure 3.9** The cumulative distribution function of OD travel time ($\boldsymbol{\alpha}$ = 30°)

Finally, based on the CDF of OD travel time obtained previously, travel time reliability between the residential area and the hospital for two given wind directions $\alpha$ = 30° and 330° are obtained with Eq. (22) and the results are given in Figure 16. Here, two acceptable threshold levels are defined: $tt = tt_0$ in level 1 and $tt = 2tt_0$ in level 2. The figure indicates that travel time reliability greatly decreases with the increase in wind speed. In addition, travel time reliability at level 2 is much higher than that at level 1. This means that a traveler wanting to arrive at the hospital from the residential area with a higher on-time probability after a strong wind event needs to plan more time for travel. It is also found that travel time reliability under wind direction $\alpha$ = 30° is higher than that under wind direction $\alpha$ = 330°, which is consistent with the connectivity results in Figure 3.9. Moreover, by comparing Figure 3.10 with Figure 3.7, it is found that under the same wind conditions the OD travel time reliability is smaller than the OD connection probability. For example, for a given wind scenario $\alpha$ = 30° and $U$ = 20 m/s, the connection probability is 0.723, while the travel time reliability is 0.435 at level 1 and 0.699 at level 2. This indicates that the travel time reliability will be equal to the connection probability when the acceptable travel time is very large.

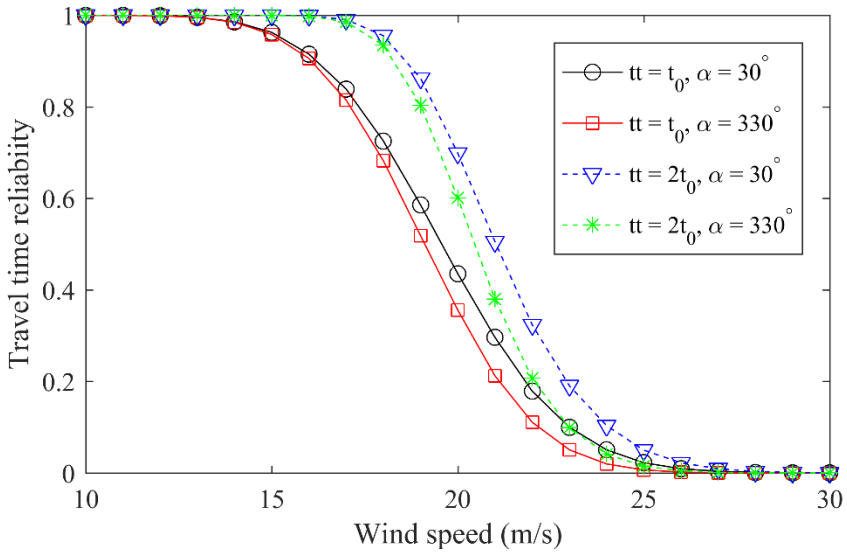


**Figure 3.10** Travel time reliability

### 3.3.4 Measures for Improving Infrastructure Performance

Removal of all vulnerable trees threatening infrastructures is neither desirable nor feasible. Crown thinning (CT) is a common measure to reduce the windthrow likelihood by reducing crown weight and wind loads acting on the crown. Usually, the extent of thinning in a year does not exceed 25% of a tree's crown. In this study, CT measure is investigated in terms of its effect on the infrastructure performance, where 25% of crown is removed for identified dangerous roadside trees in the transportation network of Fort Collins. We assume the crown density and effective crown area will be reduced by 25%, and other tree parameters will stay the same after CT. As a result, there will be a 25% reduction in both crown weight and wind loads acting on the crown. Furthermore, the windthrow fragility of trees will be affected by the reduced crown weight and wind loads. Figure 3.11 gives the breakage and uprooting fragility curves for American basswood with a height of 15-17 m before and after CT. It is found that both the breakage and uprooting fragility can be improved significantly after CT. Moreover, the effects of CT on infrastructure performance, such as powerline disruption, road closure, OD connectivity, and OD travel time reliability, are investigated. Figure 3.12 shows the disruption probability of powerline and road closure probability of link 8 under north winds ($\alpha$ = 360°). Figure 3.13 shows the disconnection probability and travel time reliability at level 2 between the hospital and the residential area under wind direction $\alpha$ = 300° before and after CT. It is observed from Figures 3.12 and 3.13 that the network performance is greatly improved after CT, as

reflected by the reduced powerline disruption probability, decreased road closure probability, reduced OD disconnection probability, and increased OD travel time reliability.

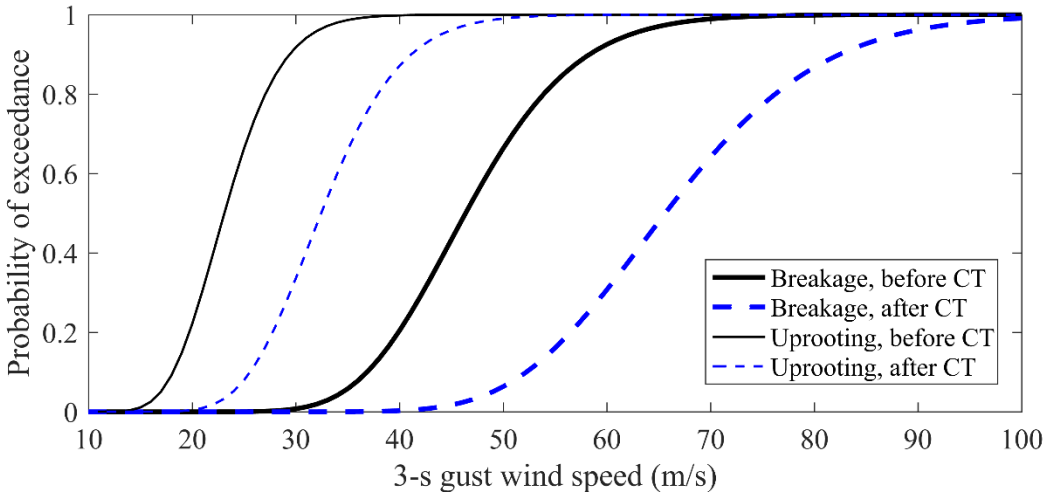


**Figure 3.11** Windthrow fragility curves for basswood before and after crown thinning

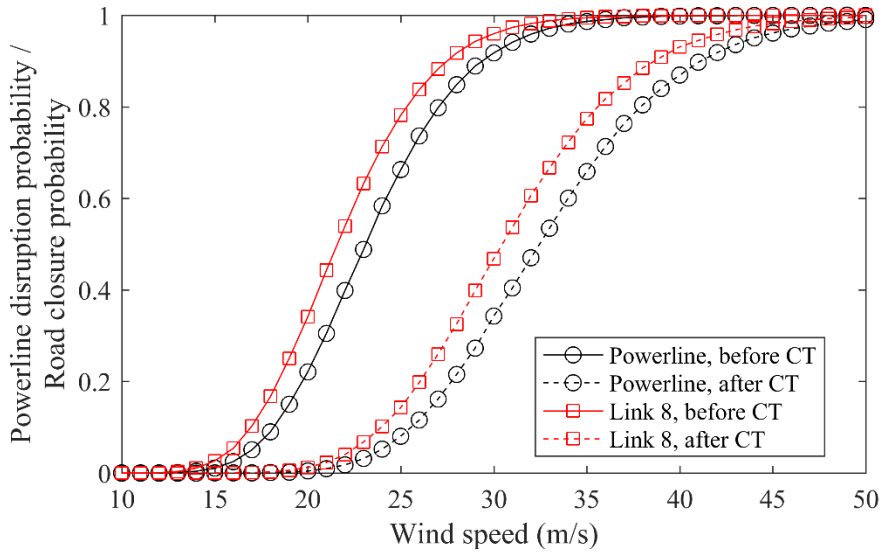


**Figure 3.12** Powerline disruption probability and road closure probability before and after crown thinning

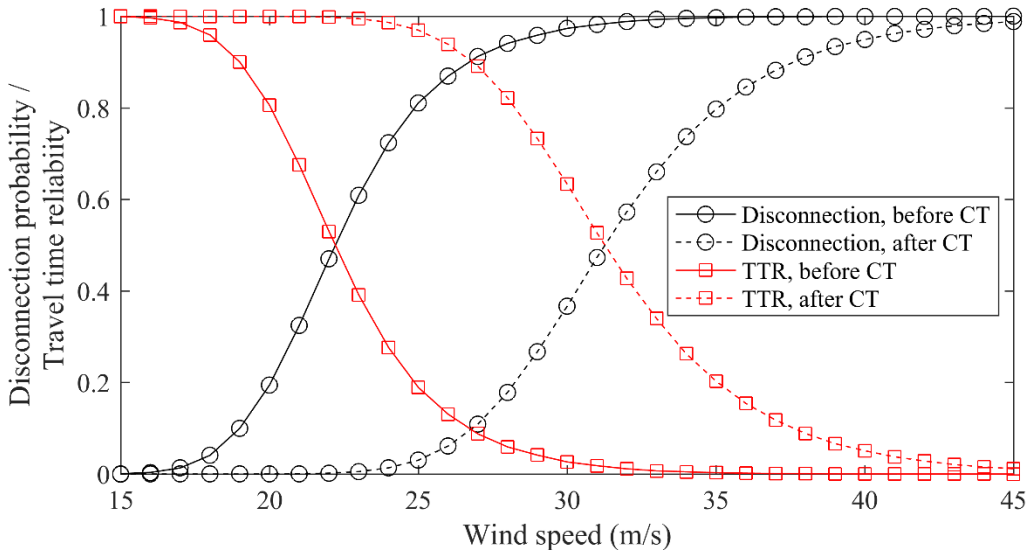


**Figure 3.13** Disconnection probability and travel time reliability before and after crown thinning

# 4. CONCLUSIONS

This study proposed a probabilistic methodology to model the disrupted infrastructures due to fallen trees during wind events. First, windthrow fragility analyses of typical urban trees under extreme winds were developed while considering the wind load uncertainties and mechanical properties of trees. An FEM-based mechanistic tree model was developed to compute the tree response subjected to wind loads. The model's basis was that both uprooting and stem breakage fragility curves of three tree species with different height classes were generated through Monte Carlo simulations. Second, the probabilistic impact on a powerline system and a transportation network is derived with the proposed framework and the MSR method by adopting the developed fragility curves. The proposed methodology was numerically demonstrated in a prototype community in the city of Fort Collins with following findings:

(1) Windthrow fragility of trees is species-dependent, which is strongly related to the wind characteristics and mechanical properties of tree species. Generally, higher stem modulus of rupture leads to lower stem breakage vulnerability, while higher critical overturning moment leads to lower uprooting vulnerability.

(2) Because species, sizes, and distributions of trees vary considerably at different locations, the powerline disruption probability, road closure probability, OD disconnection probability, and travel time reliability under strong winds were found to be sensitive to wind directions. To reduce the wind risk, the city should pay attention to vulnerable trees along powerlines and links that are nearly perpendicular to prevailing wind directions.

(3) Crown thinning of trees was found to be an effective measure to improve infrastructure performance by reducing the probability of powerline disruption, road closure, and OD disconnection and increasing the OD travel time reliability.

(4) Although demonstrated only on overhead powerline and transportation systems in detail, the proposed methodology can be extended to the performance assessment of other disrupted infrastructures related to windthrow of trees in wind events, such as underground pipeline systems and buildings once their potential vulnerability posed by fallen trees has been appropriately characterized. In this demonstrative study, three typical urban tree species were studied in terms of fragility curves. The same procedure of conducting tree fragility analysis and disruption modeling can be easily applied to other tree species and communities by considering site-specific tree, wind, and network conditions.

# REFERENCES


Ai, X. Q., Cheng, Y. Y., and Peng, Y. B. (2016). "Nonlinear dynamics and failure wind velocity analysis of urban trees." *Wind and Structures*, 22(1), 89-106.

Ancelin, P., Courbaud, B., and Fourcaud, T. Y. (2004). "Development of an individual tree-based mechanical model to predict wind damage within forest stands." *Forest Ecology and Management*, 203(1-3), 101-121.

Anderson Jr, J. D. (2010). *Fundamentals of Aerodynamics*, Tata McGraw-Hill Education.

Argyroudis, S., Selva, J., Gehl, P., and Pitilakis, K. (2015). "Systemic Seismic Risk Assessment of Road Networks Considering Interactions with the Built Environment." *Computer-Aided Civil and Infrastructure Engineering*, 30(7), 524-540.

Chisolm, E. I., and Matthews, J. C. (2012). "Impact of hurricanes and flooding on buried infrastructure." *Leadership and Management in Engineering*, 12(3), 151-156.

Ciftci, C., Arwade, S. R., Kane, B., and Brena, S. F. (2014). "Analysis of the probability of failure for open-grown trees during wind storms." *Probabilistic Engineering Mechanics*, 37, 41-50.

Cotton, W. R., Weaver, J. F., and Beitler, B. A. (1995). "An Unusual Summertime Downslope Wind Event in Fort-Collins, Colorado, on 3 July 1993." *Weather and Forecasting,* 10(4), 786-797.

Cucchi, V., Meredieu, C., Stokes, A., Berthier, S., Bert, D., Najar, M., Denis, A., and Lastennet, R. (2004). "Root anchorage of inner and edge trees in stands of Maritime pine (Pinus pinaster Ait.) growing in different podzolic soil conditions." *Trees – Structure and Function*, 18(4), 460-466.

Dupuy, L., Fourcaud, T., and Stokes, A. (2005). "A numerical investigation into the influence of soil type and root architecture on tree anchorage." *Plant and Soil*, 278(1-2), 119-134.

Duryea, M., and Kampf, E. (2007). "Wind and Trees: Lessons Learned from Hurricanes." University of Florida FOR-118, Gainesville.

Gardiner, B., Peltola, H., and Kellomaki, S. (2000). "Comparison of two models for predicting the critical wind speeds required to damage coniferous trees." *Ecological Modelling*, 129(1), 1-23.

Goretti, A., and Sarli, V. (2006). "Road network and damaged buildings in urban areas: Short and long-term interaction." *Bulletin of Earthquake Engineering*, 4(2), 159-175.

Horácek, P. (2003). "Introduction to Tree Statics & Static Assessment." *Tree statics and dynamics seminar, interpreting the significance of factors affecting tree structure & health.* Westonbirt, UK.

Kang, W. H., Song, J. H., and Gardoni, P. L. (2008). "Matrix-based system reliability method and applications to bridge networks." *Reliability Engineering and System Safety*, 93(11), 1584-1593.

Kocatepe, A., Ulak, M. B., Kakareko, G., Ozguven, E. E., Jung, S., and Arghandeh, R. (2018). "Measuring the accessibility of critical facilities in the presence of hurricane-related roadway closures and an approach for predicting future roadway disruptions." *Natural Hazards*, 1-21.

Laefer, D. F., and Pradhan, A. R. (2006). "Evacuation route selection based on tree-based hazards using light detection and ranging and GIS." *Journal of Transportation Engineering, Part A: Systems*, 132(4), 312-320.

Lavoie, S., Ruel, J. C., Bergeron, Y., and Harvey, B. D. (2012). "Windthrow after group and dispersed tree retention in eastern Canada." *Forest Ecology and Management*, 269, 158-167.

McPherson, E. G., van Doorn, N. S., and Peper, P. J. (2016). "Urban tree database and allometric equations." *General Technical Report PSW-253*, U.S. Department of Agriculture, Forest Service, Pacific Southwest Research Station, Albany, CA.

Mitchell, J. K., Devine, N., and Jagger, K. (1989). "A Contextual Model of Natural Hazard." *The Geographical Review*, 79(4), 391-409.

Peltola, H., Kellomaki, S., Vaisanen, H., and Ikonen, V. P. (1999). "A mechanistic model for assessing the risk of wind and snow damage to single trees and stands of Scots pine, Norway spruce, and birch." *Canadian Journal of Forest Research*, 29(6), 647-661.

Peper, P. J., Alzate, C. P., McNeil, J. W., and Hasherni, J. (2014). "Allometric equations for urban ash trees (Fraxinus spp.) in Oakville, Southern Ontario, Canada." *Urban Forestry and Urban Greening*, 13(1), 175-183.

Poulos, H. M., and Camp, A. E. (2010). "Decision Support for Mitigating the Risk of Tree Induced Transmission Line Failure in Utility Rights-of-Way." *Environmental Management*, 45(2), 217-226.

Poulos, H. M., and Camp, A. E. (2011). "Mapping Threats to Power Line Corridors for Connecticut Rights-of-Way Management." *Environmental Management*, 47(2), 230-238.

Ross, R. J. (2010). *Wood Handbook: Wood as an Engineering Material.*

Simu, E., & Miyata, T. (2006). *Design of buildings and bridges for wind a practical guide for ASCE-7 standard users and designers of special structures.* John Wiley & Sons.

Westfall, J. A., and Scott, C. T. (2010). "Taper Models for Commercial Tree Species in the Northeastern United States." *Forest Science*, 56(6), 515-528.

Zanini, M. A., Faleschini, F., Zampieri, P., Pellegrino, C., Gecchele, G., Gastaldi, M., and Rossi, R. (2017). "Post-quake urban road network functionality assessment for seismic emergency management in historical centres." *Structure and Infrastructure Engineering*, 13(9), 1117-1129.